Proceedings of the
Annual Stability Conference
Structural Stability Research Council
Baltimore, Maryland, April 10-13, 2018

Numerical and Experimental Studies for the Development of Direct Strength Design Rules for Locally and Globally Slender Hollow Sections

Andrea Toffolon[1] and Andreas Taras[2]

Abstract
This paper discusses the strength and stability of slender hollow sections with flat faces and different cross-sectional geometries in terms of the “Overall Interaction Concept” (OIC). The results shown are developed in the framework of the European (RFCS) research project HOLLOSSTAB. The paper focuses primarily on the behavior of bespoke cross-sections with stiffened faces respectively mono-symmetric cross-section. This allows for a more general verification of the general viability of OIC-type design rules for the direct strength design of hollow sections of general shape and material. The scope of the study consists of an extensive experimental campaign, coupled with a comprehensive series of numerical tests. The initial discussion of the results in terms of the OIC approach highlights its challenges and potential.

1. Introduction

The cross-sectional strength of hollow sections of conventional (rectangular, circular) or more general shape is determined in most international design codes (see. e.g. the Eurocode - EN 1993-1-1 or the AISC specifications) by the introduction of cross-sectional classes, whereby the full plastic capacity is postulated to be available for classes 1 and 2 (compact sections), while the elastic resistance is available in class 3 (semi-compact sections); finally, slender sections (class 4) cannot nominally develop the yield strength in any compressed fiber. This classification approach usually leads to sharp drop-offs of strength at the borders of the classes. This paper represents a progress report on on-going work within the European research project “HOLLOSSTAB”, during which alternative, new design rules for hollow sections with innovative shapes and/or steel grades are being developed on the basis of an “Overall Interaction Concept” (OIC).

This concept – similarly to the Direct Strength Method (DSM) used in North America (Schafer, 2008) for the design of cold-formed steel open cross-sections – makes use of the results of (numerical) linear buckling analyses (LBA) and materially nonlinear (plastic collapse) analyses (MNA) for the whole member to determine the slenderness and consequently an “overall”

[1] Graduate Research Assistant, Bundeswehr University Munich, <andrea.toffolon@unibw.de>
[2] Professor of Steel Structures, Bundeswehr University Munich, <andreas.taras@unibw.de>

buckling reduction factor. It eliminates the necessity for the definition of classes in cross-sectional design checks, as it leads to a continuous definition of strength as a function of an "overall" slenderness, which may include various load cases and - potentially - buckling cases. This paper describes an extensive experimental and numerical test campaign and discusses how this approach fits into the general framework of buckling design checks for hollow sections.

After a section dedicated to the scope of the study and the methodology employed, a more in-depth description of the OIC framework is given. This is followed by a description of the experimental test results and the calibration of the numerical model employed further in an extensive parametric study. The results of this study are finally discussed in the OIC context, and the encountered challenges and observed advantages of the methodology are illustrated.

2. Scope and Methodology

The strength and stability of hollow sections of various shapes and steel grades are being studied within the scope of the European research project HOLLOSSTAB by means of an extensive experimental and numerical test campaign and parametric study. This section of the paper describes the scope and methodology of the first, main series of tests and numerical analyses conducted at the Chair of Steel Structures of Bundeswehr University Munich.

2.1 Types of studied cross-section and materials

Two distinct types of cross-section are the subject of study during the HOLLOSSTAB project and are illustrated in *Figure 1*:

i. standard-shape circular (CHS) and rectangular (SHS, RHS) hollow sections produced in accordance with the European fabrication standards EN 10210 and EN 10219, which apply to hot-finished and cold-formed sections, respectively. The general dimensions and shapes for this type of section are shown in *Figure 1c and d.*

ii. cold-formed and welded sections of bespoke, stiffened shape, produced primarily for storage racking applications by *voestalpine Finaltechnik Krems GmbH* in Krems, Austria. The two shapes studied within the scope of this paper are designated VHPS ("S" for "stiffened") and VHPT ("T" for T-shaped) and are shown in *Figure 1a and b.*

The special shape of the VHPS and VHPT sections was chosen by the manufacturer to increase the local buckling strength and reduce material consumption for a given (maximum) exterior dimension, which is equal to 140mm in the studied sections. Due to their unusual shape, these types of section are of particular interest for the development of a generally valid, OIC-based method for the design of hollow sections. For this reason (as well as space limitations), in the remainder of this paper only these sections will be further considered.

The VHPS and VHPT sections that were experimentally investigated in the laboratory of Bundeswehr University were made of S355 steel (with a nominal yield strength of f_y=355 N/mm²). Tensile coupons were extracted from various locations in the section and tested in a Zwick-Roell universal test rig. While not shown in detail here, average measured yield stress values of f_y=400 N/mm² and an ultimate tensile stress f_u of 550 N/mm² were obtained. The studied sections had thicknesses of either 2,5 or 3,5 mm. In the first series of tests, described in this paper, it was decided to isolate local and distortional (stiffener) buckling effects from global buckling. For this reason, a globally rather stocky member length of 800mm was chosen.

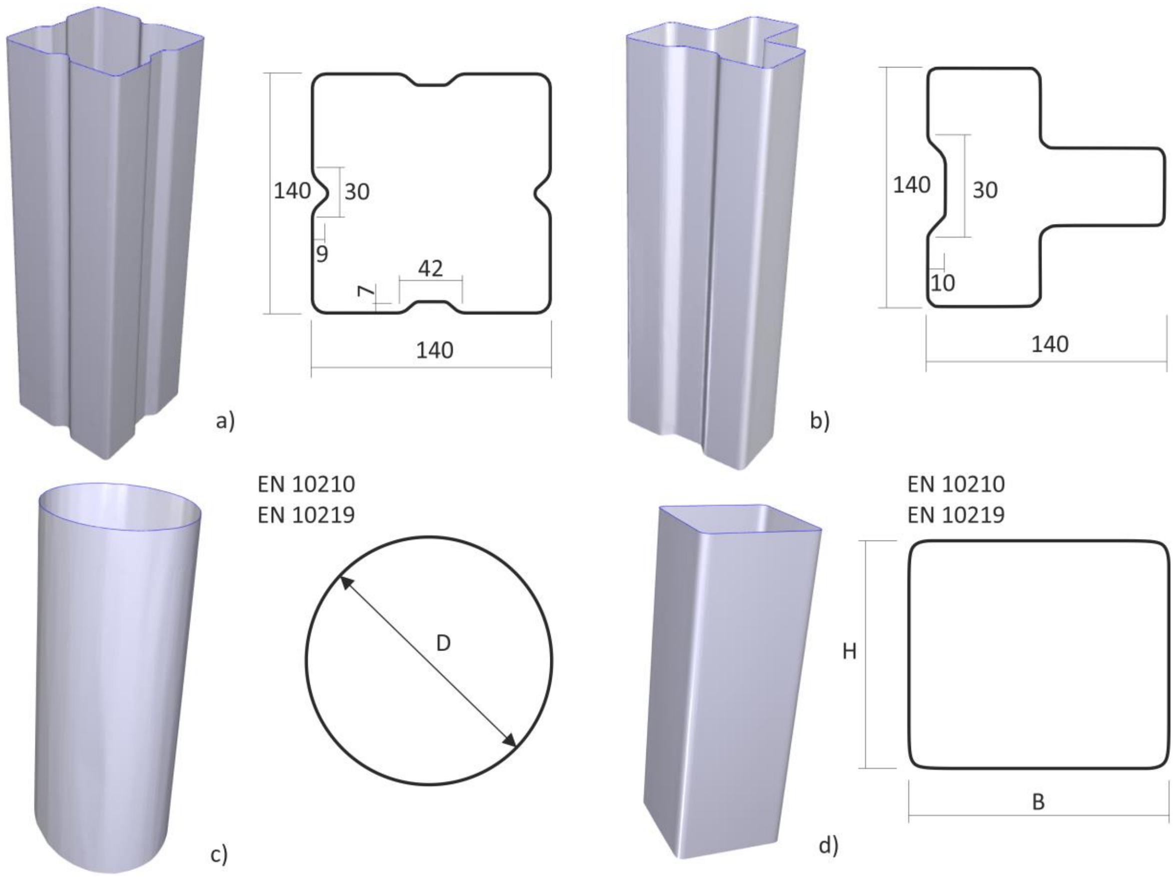

Figure 1: Section types studied at Bundeswehr University Munich: a) “VHPS”; b) “VHPT”; c) CHS; d) RHS and SHS

2.2 Experimental methodology and test campaign

A total of 16 full-scale tests were carried out on VHPS or VHPT sections of short length (L=800mm), with varying wall thicknesses and load eccentricities. These tests were carried out in the 10MN 4-column test rig in the laboratory of Bundeswehr University Munich. Stub column tests were carried with a centric load application (in the centroid axis, determined analytically in the case of the VHPT section). The bending moment was introduced by adding eccentricity to the test specimen by employing a stiff lever arm plate. *Figure 2b and c* illustrate the employed experimental loading scheme.

The overarching aim of the experimental test campaign is to obtain a reliable basis for the calibration of numerical (FEM-based) simulations of an even wider set of load parameters and cross-sectional configurations. The simulation of the experiments thus employs a process of reverse engineering which is based on the real geometry of the specimen, as well as the measured stress-strain curve of the material, in the FEM modelling of the experimental tests.

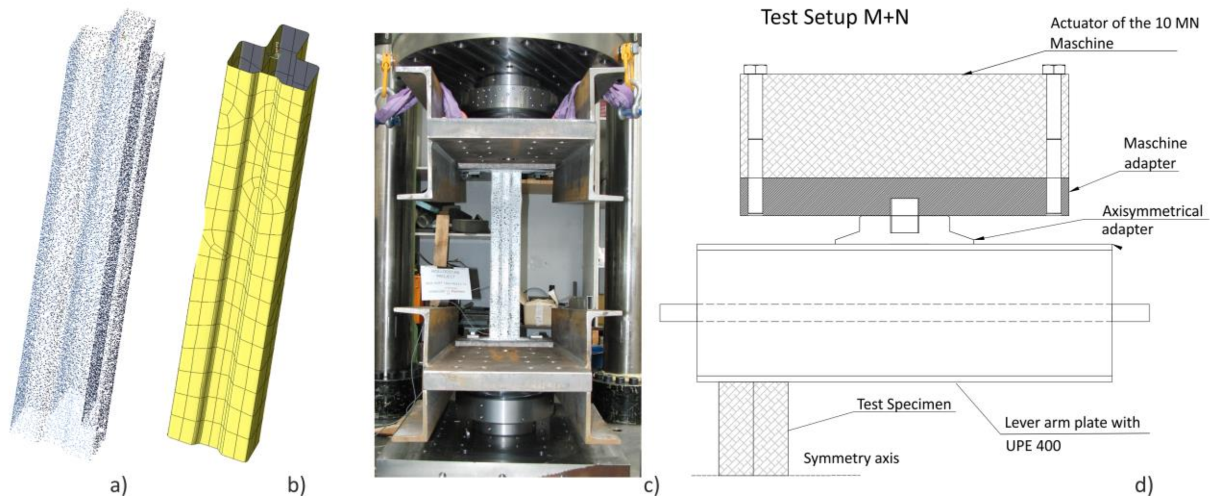

Figure 2: a) point cloud of the 3D scan data; b) spline curves approximating the real geometry c) experimental test in the 10 MN test rig; d) schematic representation (side view) of the test setup.

To facilitate this, each specimen's geometric shape and the shape deviations from the ideal geometry have been measured with a 3D scanning system made by Zeiss©. 3D spline curves were laid over the point cloud obtained from the 3D scan and imported into the finite element simulation.

Furthermore, in order to obtain an as-far-as-possible complete overview of the full deformation field in the specimen during the test (before and after local buckling occurred), a DIC (Digital Image Correlation) measurement system was employed, see *Figure 2a*. At each test time step (consistent with the experimental test duration) two pictures were taken with GOM Aramis high-resolution cameras, as the basis for the derivation of the deformations and local strains in a randomly applied speckle field on the specimens.

2.3 Numerical methodology and campaign

The mentioned reverse engineering process consists in replicating the experimental test in a "numerical test", i.e. in a geometrically and materially non-linear analysis on the imperfect geometry (GMNIA), with the highest possible accuracy. A GMNIA analysis with the measured geometrical shape of the sections and material law can lead to minimum (<3%) deviations to the ultimate load of the buckling tests if the meshing and modelling of boundary conditions is accurate. This type of GMNIA analysis is denoted by "GMNIA-MEAS" in the present paper.

The comparison between the "GMNIA-MEAS" and the experimental test results allows for a fine-tuned calibration of generalized, somewhat simpler FEM-models, which may then be used in a broader parametric study. DIC data was used in order to compare both the global shortening and the local deformation and buckling phenomena in the numerical and experimental tests, see *Figure 3*.

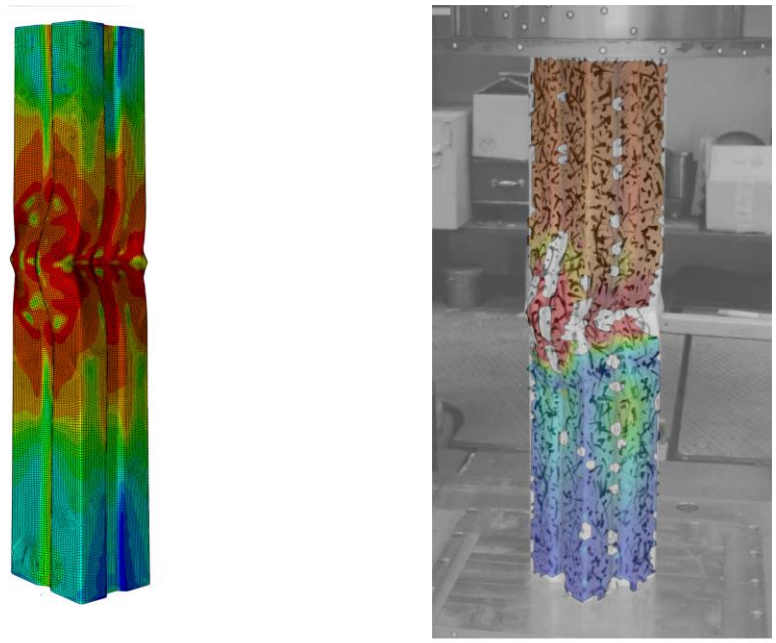

a) b)

Figure 3: a) deformed shape of a VHPS stub-column test of a GMNIA-MEAS numerical analysis with Abaqus; b) specimen deformed shape of the corresponding experimental test measured by the Aramis system.

In this calibration, the first step consists in the determination of the mesh density, element type and boundary conditions that best describe the experimental test, provided that the geometry and material law are precisely modelled. In the main step, a simpler, more generalized model, with a simplified definition of the material law and the geometrical imperfections, yet the same FEM mesh size and element types as the ones validated through the calibration to the experimental tests. The main simplification thus consists in the determination of an *equivalent* imperfection shape for the GMNIA calculation. In the study presented in this paper, the imperfect geometry was derived from the first buckling mode of a Linear Buckling Analysis (LBA), with the amplitude for the buckling waves calibrated as described in section 4. This procedure is schematically represented in *Figure 4a* and *b.*

Concerning the stress-strain relationship, three different models were applied in the present paper, see *Figure 4c*: *i.* for the “GMNIA-MEAS” used for the model calibration, the stress-strain curve from the tensile test was used; *ii.* a stress-strain curve with linear material hardening was used to calibrate the equivalent imperfection amplitude: in this case, an LBA analysis was used to determine the imperfect shape, while a GMNIA analysis with material hardening was used for the calibration. The strain-stress curve with hardening is doubly linear, with a slope equal to E=210,000 N/mm² up until f_y and equal to E/100 in the non-elastic portion; *iii.* finally, for the parametric study, an ideal plastic stress-strain curve was used, as it was noticed that the linear strain hardening did not noticeably alter the numerical results in terms of ultimate buckling load, which was the main parameter of interest in the case of the parametric study.

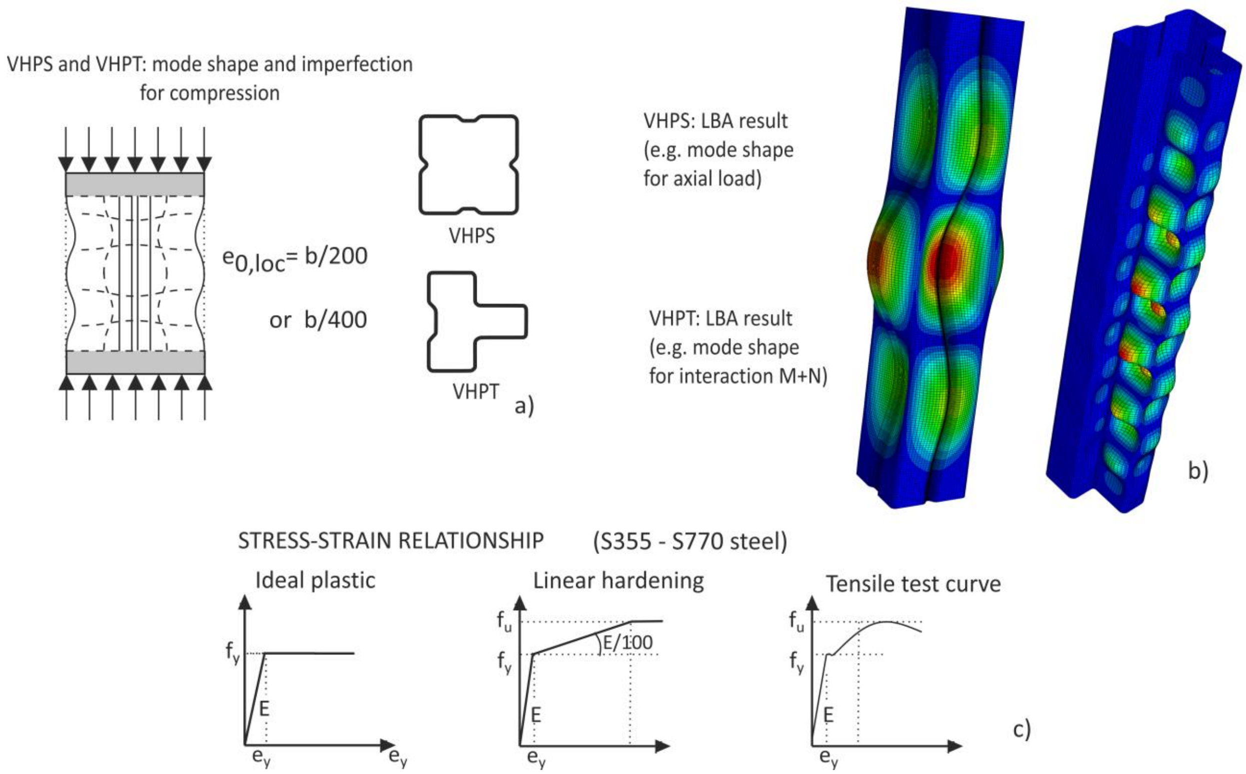

Figure 4: a) representation of the imperfection and mode shape from the LBA analysis;
b) Example of LBA results for the analyzed cross-sections
c) Three different stress-relationship used in the numerical simulations.

The proprietary software Simulia ABAQUS was used for all numerical simulations, with linear isoparametric shell elements with reduced integration (element type S4R). As a result of the model calibration, it was found that a mesh density with 60 elements in circumferential and 200 elements in longitudinal direction was sufficient to obtain results with an average difference between the "GMNIA-MEAS" and the experimental test result of less than 3% in terms of ultimate buckling load.

3. The OIC framework

In the European research project HOLLOSSTAB, the Overall Interaction Concept (OIC) (*Boissonnade et al., 2016*) is used as the main reference framework and representation tool for the analysis, representation and design method of calibration for the resistance of both members and cross-sections. This concept, similarly to the DSM (Direct Strength Method) developed in North America for the design of cold-formed sections (*Schaefer, 2008*), makes use of a generalized, "overall" definition of slenderness and of the buckling reduction factor in order to define the ultimate buckling capacity of cross-sections and members failing in local (L), distortional (D), global (G) or interactive (I) buckling.

In this paper, only local buckling (coupled with some distortional effects) are being considered. Therefore, only the overall slenderness $\bar{\lambda}_L$ for local buckling, as well as the corresponding buckling knock-down factor χ_L, will be presented and discussed in the following.

The OIC adopts a series of steps, which are illustrated graphically in *Figure 5* and are described in the following:

i. the first step of the OIC method consists in the calculation of the plastic resistance at a local, cross-section level ($R_{pl,L}$), defined as an amplification factor for a given load state. This may e.g. be pure compression or bending, or a combination thereof.

ii. in the next step, the critical, elastic bifurcation load is calculated (R_{cr}), for example $R_{cr,L}$ for local buckling, either by available analytical methods or (more commonly) by numerical analysis, as the first (local) buckling eigenvalue in an LBA analysis.

iii. the third step consists in the calculation of the corresponding overall slenderness:

$$\bar{\lambda} = \sqrt{\frac{R_{PL}}{R_{cr}}} \tag{1}$$

iv. finally, in a fourth step, a buckling knock-down factor χ_L may be determined from previously derived and validated design formulae, and applied to the plastic resistance R_{pl} to obtain the ultimate buckling resistance R_b - termed $R_{b,L}$ in the case of the resistance against local buckling.

The determination and validation of these formulae is the main task and challenge in the development of OIC-type design methods, and may be seen as the main objective of the HOLLOSSTAB project for the application case of hollow sections.

Figure 5a shows the four above-mentioned steps in the common $\bar{\lambda}$-χ diagram format. The individual variables R_{pl}, R_{cr}, χ and R_b are illustrated within an M-N interaction diagram in *Figure 5b*, where normalized bending moments m and axial forces n are used. Since the OIC method consistently makes use of load amplification factors, a given load case is more generally described by a "loading angle" ϕ, which is equivalent to:

$$\phi = arctg(m/n) \tag{2}$$

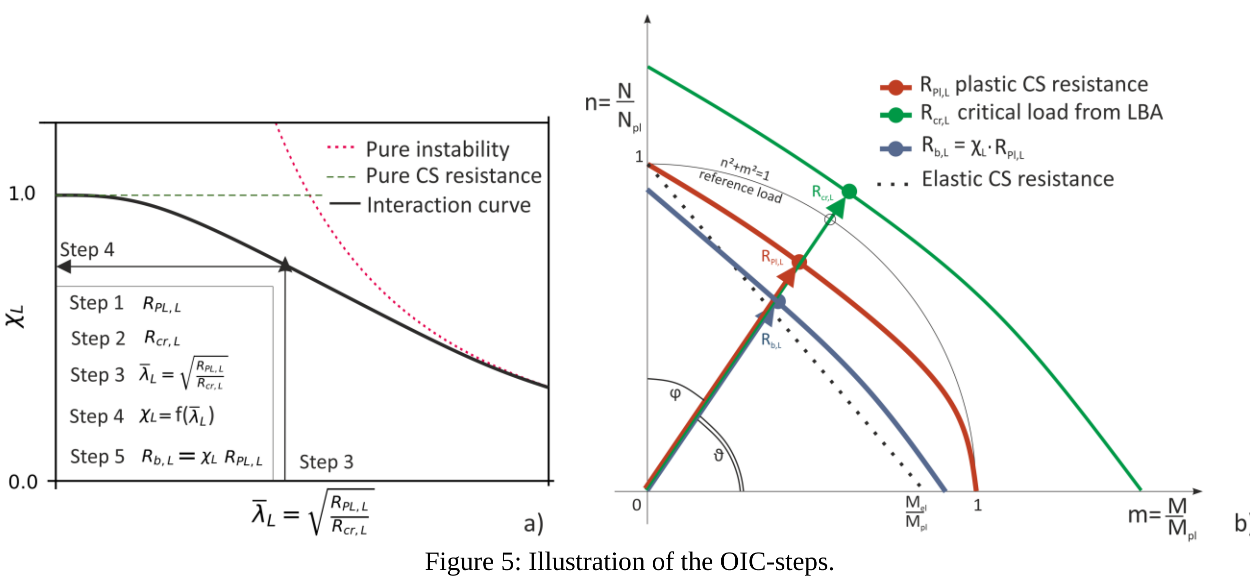

Figure 5: Illustration of the OIC-steps.

4. VHPS and VHPT sections - experimental test results and numerical model calibration

4.1 Overview of test results

A synthetic overview of the experimental test results, which were carried out as described in section 2 of this paper, is given in *Table 1*. Thereby, the eccentricity “e” determines the amount of bending. It was applied in direction of the “web” of the VHPT sections, and so as to cause additional compression on the wider stiffener in the VHPS sections. The numbering indicated in the table followed the overall progress of the project’s test campaign.

Table 1: Experimental test results for the bespoke Cross-sections.

Specimen No.	Cross-section type	B [mm]	H [mm]	T [mm]	L [mm]	e [mm]	$F_{Exp,max}$ [kN]
8	VHPS	140	140	2,5	800	0	623,9
9	VHPS	140	140	2,5	800	15	614,8
10	VHPS	140	140	3,5	800	0	1002,4
11	VHPS	140	140	3,5	800	15	995,9
13	VHPT	140	140	3,5	800	10	1106,9
12	VHPT	140	140	3,5	800	0	1099,2
14	VHPT	140	140	2,5	800	0	584,5
15	VHPT	140	140	2,5	800	10	594,3
16	VHPS	140	140	2,5	800	137	208,2
17	VHPS	140	140	2,5	800	314	99,0
18	VHPS	140	140	3,5	800	91	328,3
19	VHPS	140	140	3,5	800	308	156,0
20	VHPT	140	140	2,5	800	195	121,1
21	VHPT	140	140	2,5	800	372	63,3
24	VHPT	140	140	3,5	800	195	224,9
25	VHPT	140	140	3,5	800	372	118,3

4.2 Calibration of the numerical model

With the chosen FEM modelling technique and discretization, described in section 2, the GMNIA-MEAS model is able to approximate the resulting maximum force of the experimental test with an error of less than 3% in terms of ultimate load. In most observed cases, the deformation curve also follows the test curve very closely, with the more significant deviations occurring in the plastic post-buckling range. As a representative example, *Figure 6a* shows the GMNIA-MEAS results for the VHPS stub-column test on specimen #8, in terms of global axial shortening, in comparison to the test results obtained from the calibrated test rig sensor and the DIC (Aramis) evaluation.

The GMNIA-MEAS load-deformation curve is then compared to different GMNIA calculations with varying *equivalent* imperfection amplitude. As described in section 2, the latter models are built from an equivalent geometry with imperfection shapes taken from an LBA analysis and a simplified stress-strain curve with linear hardening. In the stress-strain curve for the material hardening, both f_y and f_u are derived from the tensile stress values.

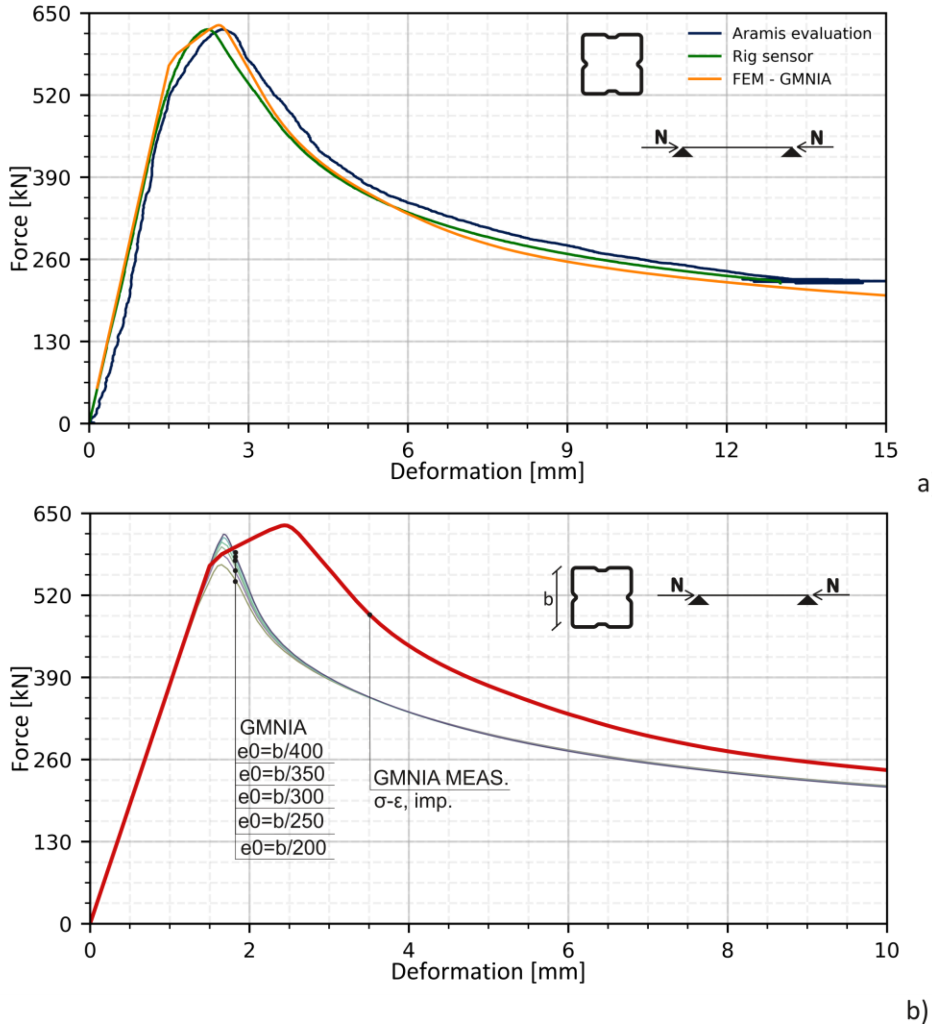

Figure 6: a) load deformation diagram of the experimental test #8 measured with DIC and traditional methods, plotted against the GMNIA-MEAS calibration model results; b) varying imperfections in GMNIA analyses plotted against the GMNIA with measured values.

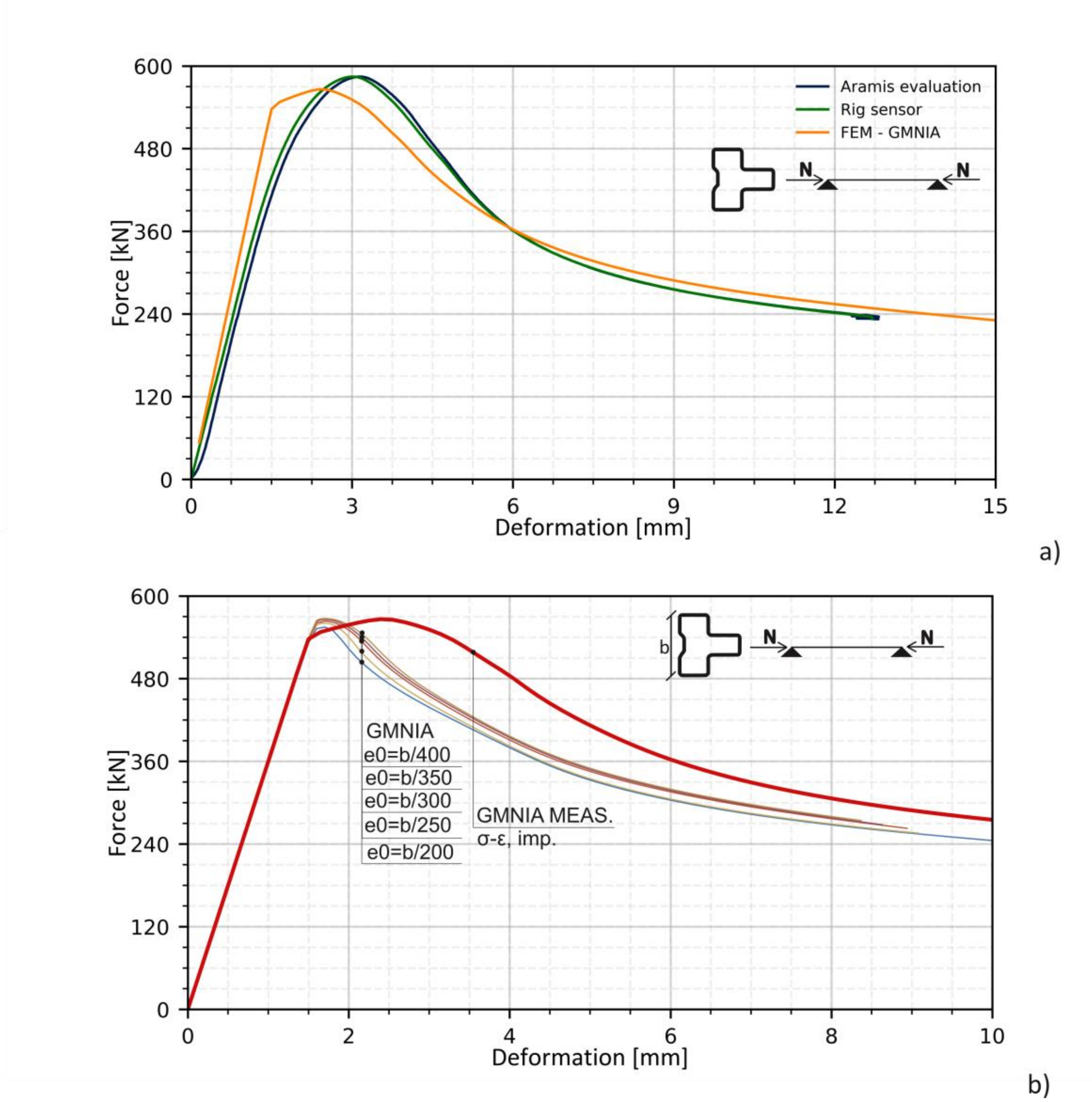

Figure 7: a) load deformation diagram of the experimental test #14 measured with DIC and traditional methods, plotted against the GMNIA-MEAS calibration model results for; b) varying imperfections GMNIA analyses plotted against the GMNIA with measured values.

Figure 7 shows the same type of evaluation for the example of a VHPT section under pure compression, specimen #14 in the test series.

The overall evaluation of the calibration work on the various tested cross-section shapes and load eccentricity values led to the conclusion that an equivalent imperfection based on the LBA first buckling mode with an amplitude b/400 is the most representative "even-numbered" value for the test series, and was thus taken to be generally more representative for the local buckling behavior of the these bespoke (and other flat-surfaced) sections than the value of e_0=b/200 contained in Eurocode design provisions (EN1993-1-5, Annex C; 2005). This is also in line with what the findings of e.g. *Lindner et al.*: they determined that amplitudes of b/400 are most suitable to represent the so-called Winter curves for local buckling in numerical analyses.

5. Numerical study and comparison with code provisions

In the remainder of this paper, some selected results from an extensive numerical study on the local buckling behavior of VHPS and VHPT sections are presented and described in detail, using the OIC framework as a tool of representation and discussion of the results.

The parametric numerical test campaign described in the following was carried out by varying and combining the following parameters:

- Thickness:
  - t=1.0 mm to t=4.0 mm with 0.5 mm step for the pure compression case
  - t=2.5 mm and t=3.5 mm for the M+N interaction and the pure bending cases.
- Length of the modelled member:
  - L=400mm
  - L=800 mm (used in most cases)
  - L=1200 mm
- Material grades (with ideal plastic material law):
  - S355 (f_y=S355 N/mm²)
  - S460 (f_y=460 N/mm²)
- Imperfection amplitudes:
  - b/400 (used in most cases)
  - b/200 (used to demonstrate the imperfection sensitivity)
- ϕ angle:
  - ϕ=0° to ϕ=90° with 10 intermediate steps in the m-n space.

In the following figures, the results of the parametric numerical study are plotted in two formats: the m-n format, which is best used to illustrate the "loss" of resistance in comparison to the full plastic capacity, and the slenderness-dependent OIC format, for which design rules are to be developed in the HOLLOSSTAB research project.

5.1 Results for VHPS sections

The local buckling behavior of VHPS sections as observed in n-m plots is illustrated for some representative examples and parameter variations in *Figure 8*. The GMNIA results are given by the dots in the figure, while the continuous lines represent reference resistances. The (ideal) plastic and elastic cross-sectional resistances are independent of code provisions, while the "N-M EC3" lines represent the simplified rules for plastic cross-sectional resistances of rectangular and square hollow sections found in Eurocode 3 (EN1993-1-1, 2005). The individual graphs can be briefly described as follows:

i. *Figure 8a* shows the influence of the (constant) wall thickness, with otherwise equal member length (L=800mm), steel grade (S355) and imperfection amplitude (e_0=b/400). As could be expected, the resistances lie between the elastic and plastic cross-sectional capacities, with the thinner cross-section getting closer the elastic (class 3) cross-section capacity line. This indicates that the producer's principal goal of obtaining sections that can be safely designed against first yield criteria is achieved for the dimensions and steel grades considered here.

ii. *Figure 8b* shows the influence of the steel grade. A higher-strength steel grade (S460) leads to a relative (but obviously not absolute) reduction of strength in comparison to the plastic cross-sectional resistance.

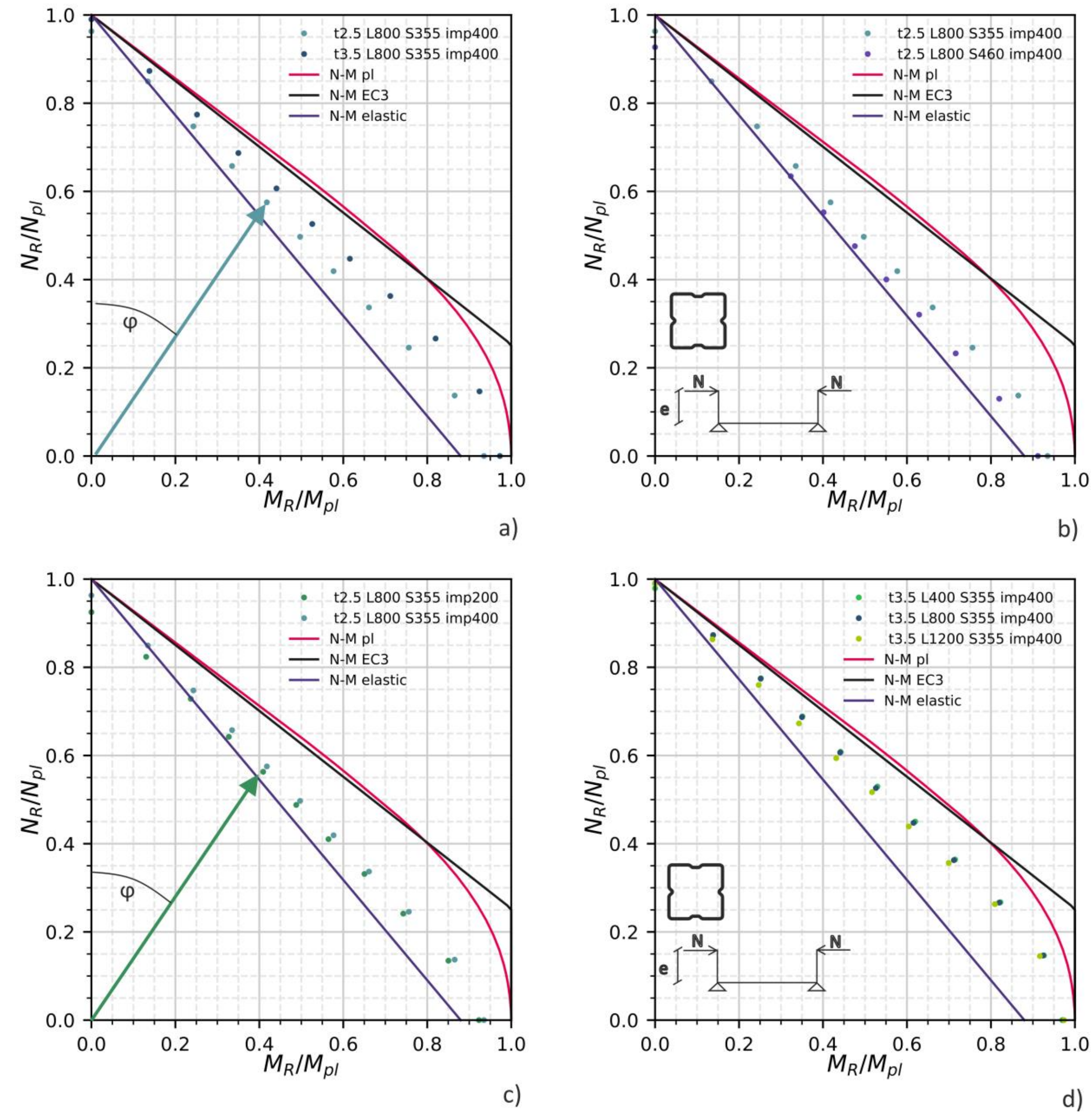

Figure 8: a) normalized bending moment plotted against normalized axial force, showing a comparison between the GMNIA results of two different b/t ratios; b) comparison between two different steel grades; c) variation of the imperfection b/400 and b/200; d) comparison of different tube lengths.

iii. The imperfection sensitivity is illustrated in *Figure 8c*. While the differences between the GMNIA results obtained for e_0=b/400 and b/200 only amount to less than 5% for the section with t=2,5mm thickness, this difference increases somewhat with greater local slenderness and is generally not negligible.

iv. Finally *Figure 8d* shows that the member length does have a small, yet not entirely insignificant effect on the local/distortional buckling behavior. This is a clear indication that distortional effects, respectively effects stemming from the buckling of the "stiffeners" in the section, are of some importance in these types of section.

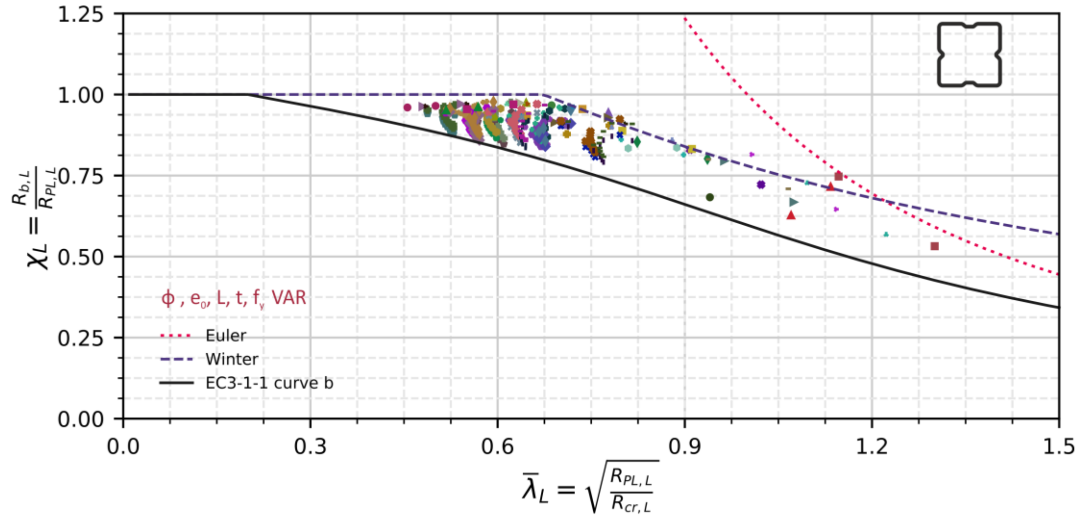

Figure 9: Overall local buckling reduction factor χ_L plotted over the generalized overall slenderness for local buckling $\bar{\lambda}_L$ for all the results of the VHPS numerical campaign.

In the following, the results for the VHPS sections are discussed in terms of their representation within the OIC framework. This is first done for all combinations of parameters described in the beginning of this section, see *Figure 9*. This plot shows all obtained GMNIA results, for various thicknesses, lengths, load cases, steel grades and imperfection amplitudes, expressed in terms of the local buckling knock-down factor χ_L (as a reduction factor to be applied to the plastic resistance $R_{pl,L}$) plotted over the overall slenderness for local buckling, $\bar{\lambda}_L$.

As can be seen in the figure, all results fall in a fairly narrow scatter band that is comprised between the Winter curve (as found in Eurocode 3 - EN 1993-1-5) and the "intermediate" column buckling curve of Eurocode 3 - EN1993-1-1, curve b.

A more detailed analysis of the obtained results was carried out for a more limited number of VHPS sections and is described in the following by referring to *Figure 10*. The results plotted in this figure can be describes as follows:

i. In *Figure 10a*, the results for three VHPS sections, each of length L=800mm and loaded at various levels of eccentricity e (corresponding to a certain angle ϕ in the n-m plot) are shown. The plot illustrates the vertical depth of the scatter of the buckling resistances resulting from the variation of the angle ϕ alone, with various values of similar OIC slenderness having OIC local buckling reduction factors χ_L that vary by around 10-15%.

ii. This behavior is illustrated further in *Figure 10b*, where the results for a specific VHPS section (t=3,5mm, S355) are plotted for various values of ϕ. The plot shows how the values of χ_L progress as the angle ϕ (and thus the load eccentricity e) increases. A curve resembling the Greek letter “γ” results, which was observed to be a quite characteristic behavior for all SHS / RHS and VHPS / VHPT types of hollow section. The lowest point of this “curve” was reached at 66° for the studied section.

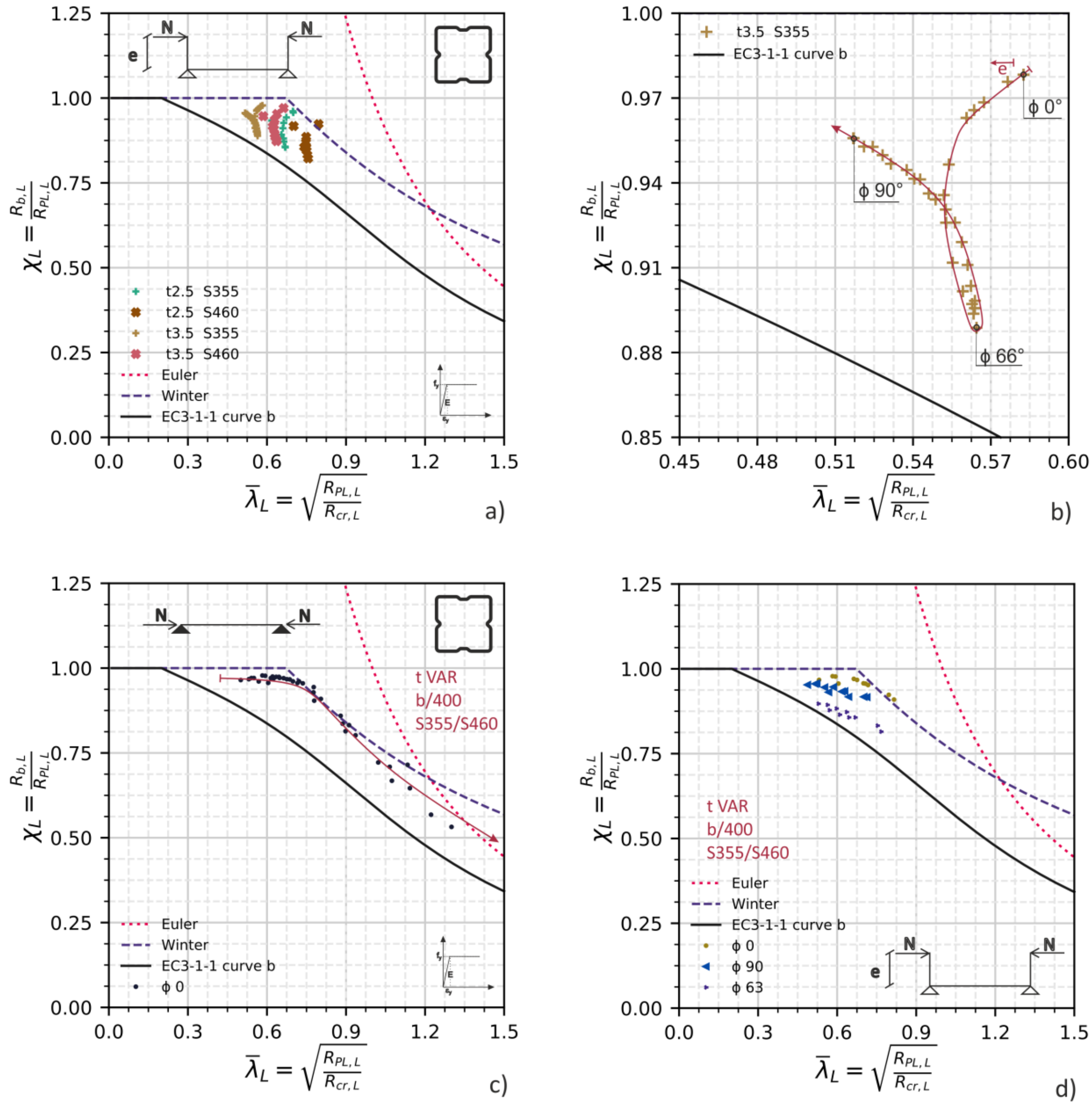

Figure 10: a) two CS and two steel grades compared varying ϕ; b) zoom of the plot (a) emphasizing the increasing eccentricity; c) varying thickness in axial force load case; d) varying thickness for the pure axial force case (ϕ=0°), pure bending moment (ϕ=90°), minimum reduction factor (ϕ=63°).

iii. *Figure 10c* shows the buckling resistances of VHPS with various steel grades and plate thicknesses (and thus slenderness values), for the case of pure compression. For this basic load case, the buckling curves follow the basic Winter curve fairly closely - as could be expected for lightly stiffened rectangular plates failing in local buckling.

iv. Finally, *Figure 10d* shows the buckling curves that result for VHPS sections of various thickness and three different levels of eccentricity. The pure bending and the pure compression results lie at a about the same level, with the bending values being 3-4% lower. At an angle ϕ of 63°, approximately 10% lower resistance values were found.

5.2 *Results for VHPT sections*

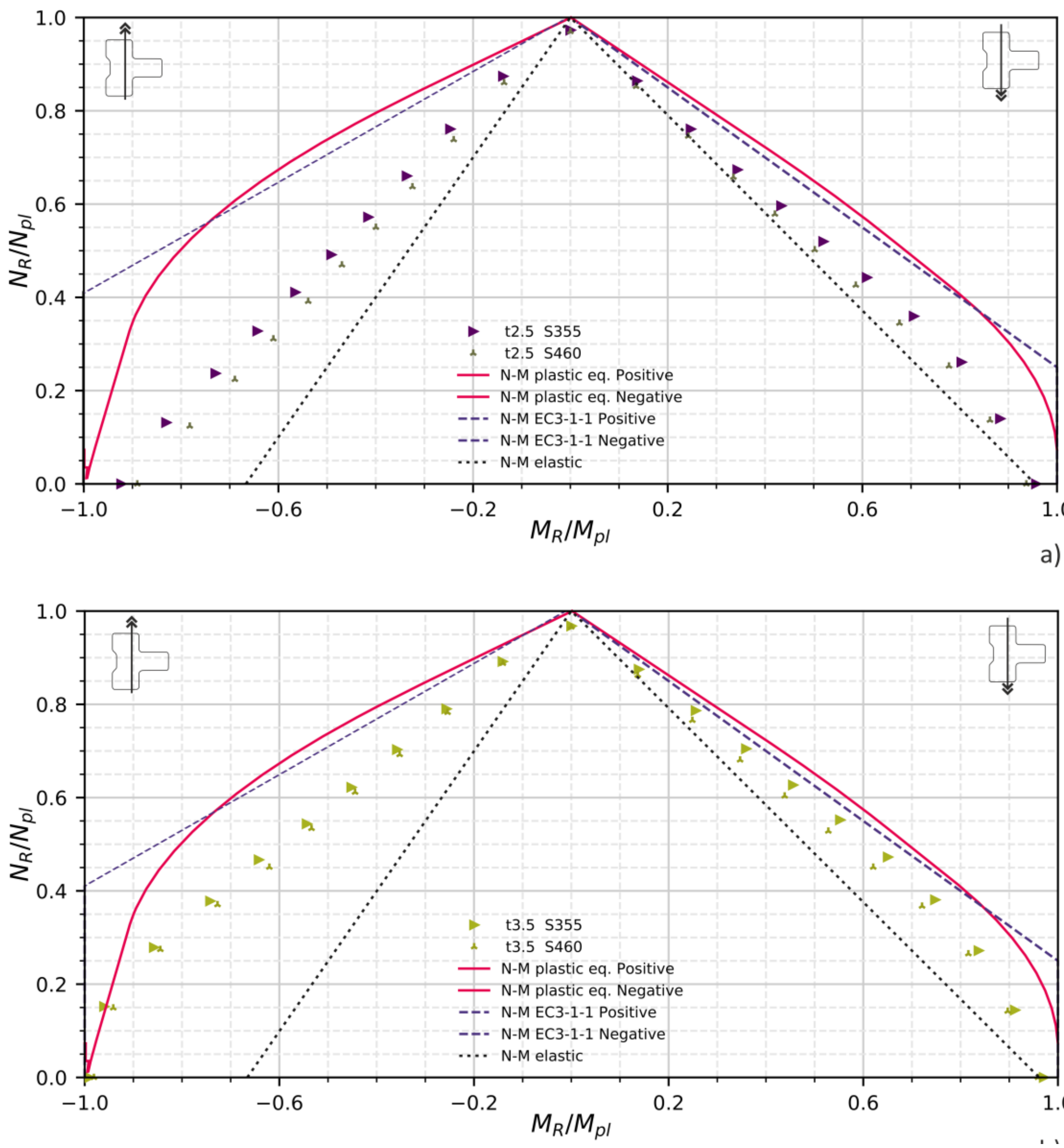

Figure 11: a) comparison between S355 and S460 for t=2.5 mm; b) comparison between S355 and S460 for t=3.5 mm.

For the VHPT cross-sections, a similar analysis was carried out, whereby in this case the direction of bending becomes relevant. This is necessary because the cross-section is not symmetric about both principal axes. The bending moment was defined as being "positive" when it caused compression on the wider (stiffened) side of the section. The determined (GMNIA) buckling resistances are shown in *Figure 11* for two exemplary VHPT sections, with *Figure 11a* showing a section with t=2.5mm thickness, while *Figure 11b* illustrates the behavior of a section with t=3.5mm wall thickness. The plastic (class 2) and elastic (class 3) resistances are shown in the plot, as well as an adapted interpretation of the EC3 rules for the N-M interaction of class 2 hollow sections. In this case, the rule (which is strictly only valid for RHS/SHS and other double symmetric sections) was evaluated by entering the width "b" of the compression flange in all calculations.

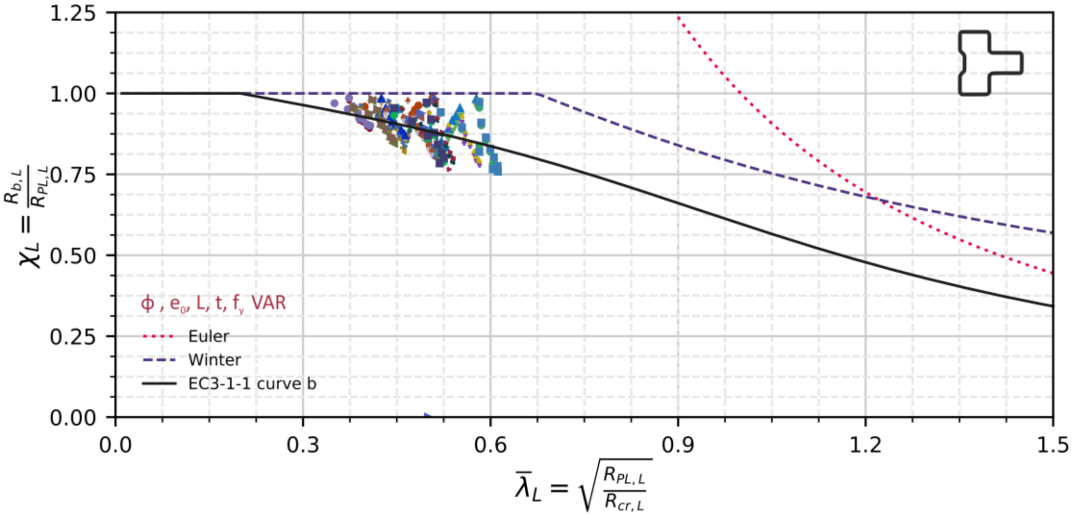

Figure 12: Results of the VHPT GMNIA numerical campaign in the OIC format.

As can be observed in *Figure 11*, the (GMNIA) buckling resistances again show a rather unsurprising behavior in the N-M plot, with the resistances varying between the elastic and plastic limits. However, particularly for negative bending, the section capacity of the more slender (t=2,5mm) section falls well below the theoretical and adapted EC3 prediction of the plastic interaction, even though the section would be classifiable as "Class 2" (compact) according to the Eurocode and other design codes, and thus plastic design could apply. In positive compression, the classification in Class 2 (compact) or Class 3 (semi-compact) is less straightforward, as the "stiffener" provides a length-dependent stiffening and thus modification of the local buckling susceptibility.

Figure 12 shows the GMNIA buckling resistance results for all examined cases of VHPT in terms of the OIC approach. The scatter band of possible results for χ_L is fairly wide, more so than in the case of the VHPS. In order to be able to better interpret these results, it is again convenient to show individual results for selected cross-sections and loading cases. this is done in *Figure 13*, which can be described as follows:

i. *Figure 13a* shows the results for a single VHPT section, of thickness t=2.5mm and length L=800mm, loaded at various levels of eccentricity e in both directions; these directions are represented separately. Similarly as in the case of VHPS sections, but in an even more pronounced way, the plot illustrates the vertical depth of the scatter of the buckling resistances resulting from the variation of the angle ϕ. Differences of up to 25% are observed, at very similar values of $\bar{\lambda}_L$.

ii. In *Figure 13b*, this behavior is illustrated further in a zoomed-in representation of the same results. Among the 10 angles analyzed, the lowest buckling knock-down factor in the OIC representation is found for 63°, which is an angle that falls close to the point where the plastic cross-sectional interaction curve diverges most from the elastic one. This appears to be the source of the drop-off in strength in the OIC representation: the fully plastic N-M resistance appears to be generally too optimistic for sections of this type.

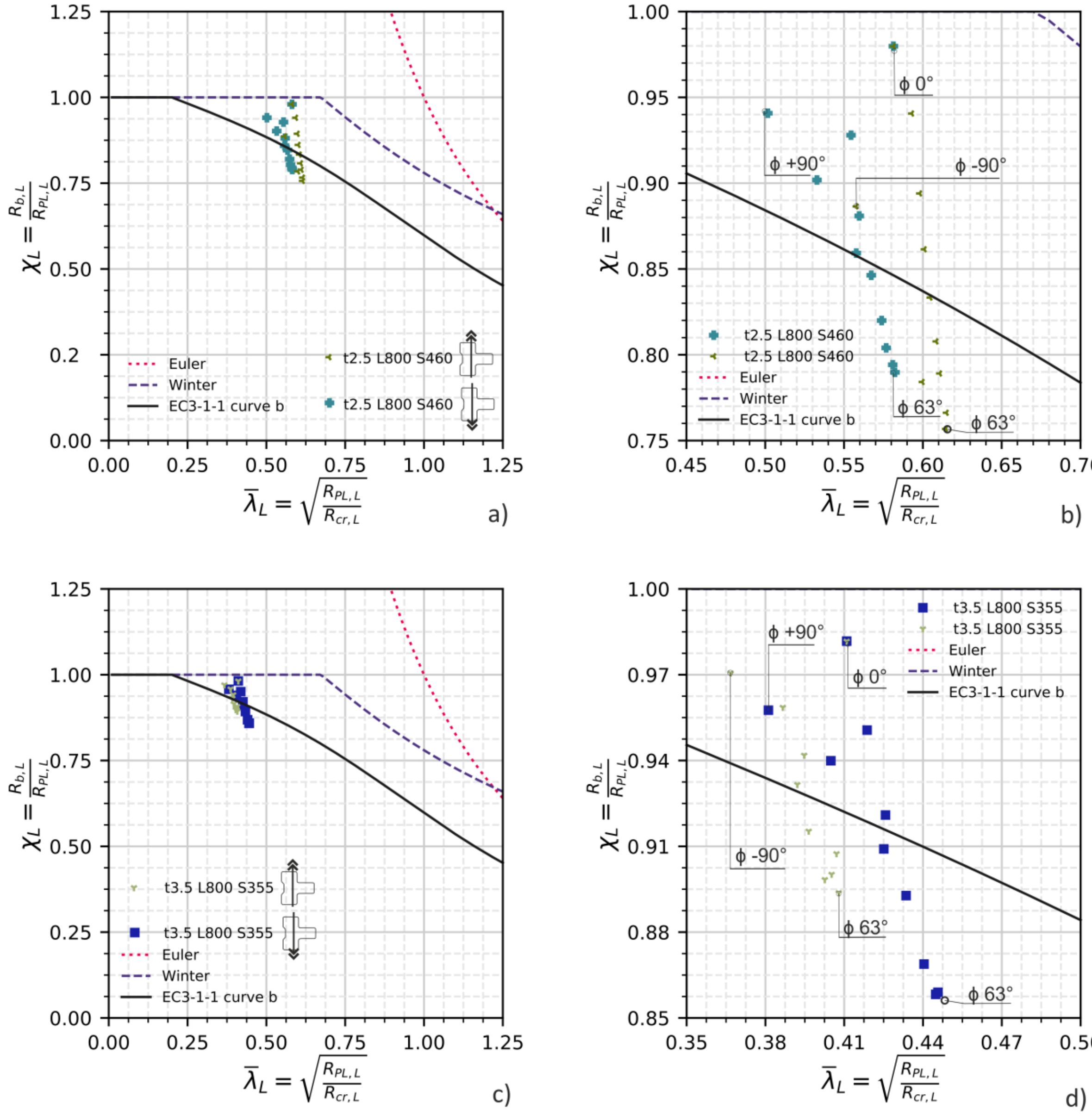

Figure 13: a) Variation of ϕ for a VHPT CS with t=2.5 mm and S460, highlighting with different markers and colors the positive and the negative bending moment; b) zoom of the plot (a) emphasizing the pure axial force load case (ϕ=0°), positive pure bending moment (ϕ=90°), and the negative pure bending moment (ϕ=90°); c) variation of ϕ for a VHPT CS with t=3.5 mm and S355; d) zoom of the plot (c).

iii. *Figure 13c* shows comparable results for the thicker section (t=3.5mm).

iv. A close-up of the same results in *Figure 13d* again shows the characteristic drop-off of strength with increasing angle ϕ, up to 63°, and the characteristic "γ" shape of the resulting curves in the OIC format

In conclusion, it can be stated that, when plotted in the OIC format, the buckling resistances of VHPS and VHPT sections reveal a certain degree of overestimation of the "base resistance" given by the fully plastic N-M interaction of these sections. This resistance level may not be appropriate as the point of reference for OIC-type buckling strength representations for this and other types of rectangular and square hollow sections.

6. Summary and Conclusions

This paper gave a progress report on on-going work within the European research project "HOLLOSSTAB", during which new design rules for hollow sections with innovative shapes and/or steel grades are developed on the basis of an "Overall Interaction Concept" (OIC). A special focus of the paper was put on the behavior of "bespoke" welded cross-sections with flat plates, i.e. sections with stiffeners and non-rectangular shape. On the basis of experimental and numerical tests, representations of the buckling strength of these sections in the OIC format were developed. These allow for an assessment of the viability of the OIC approach for the design of general hollow sections of various steel grades.

The next steps of the project will consist in the further development of initial OIC-type design rules for hollow sections of more general shape.

Acknowledgments

The authors would like to acknowledge the funding received by the European Community's Research Fund for Coal and Steel (RFCS) under grant agreement No. 709892 - HOLLOSSTAB. Additionally, the authors express their gratitude to the engineering department of *voestalpine Krems Finaltechnik GmbH*, in particular to Mr. P. Häckel, for the contributions and technical support provided during the study on VHPT and VHPS sections.

References

EN 1993-1-1, "Eurocode 3. Design of steel structures – Part 1-1: General rules and rules for buildings", *CEN* - European Committee for Standardization, Brussels, 2005

ANSI/AISC 360-10, "Specification for Structural Steel Buildings", American Institute of Steel Construction, Chicago (IL), 2010.

N. Boissonnade, J. Nseir, E. Saloumy, "Use of the Overall Interaction Concept for the practical design of steel sections and members", Proc. 5th Int. Conf. SEMC, Cape Town, 2013.

Schafer, B.W., "Review: The Direct Strength Method of cold-formed steel member design", Journal of Constructional Steel Research, Vol. 64, Issue 7-8, pp. 766-778, Elsevier, 2008.

EN 10210 "Hot finished structural hollow sections of non-alloyed and fine grain", CEN – European Committee for Standardization, Brussels, 2006.

EN 10219 "Cold formed welded structural hollow sections of non-alloy and fine grain steels", CEN – European Committee for Standardization, Brussels, 2006